Assessment of Ionospheric Models for GNSS during a Year of Solar Maximum

A. Rovira-Garcia, J.M. Juan, J. Sanz, G. González-Casado, D. Ibáñez and J. Romero-Sánchez
Research group of Astronomy and Geomatics (gAGE) at the Technical University of Catalonia (UPC)
Jordi Girona, 1-3, 08034, Barcelona, Spain

BIOGRAPHIES

Mr. Adrià Rovira-Garcia received his Aerospace Engineering degree in March 2010 from the UPC, Spain. He is currently pursuing a PhD in the Aerospace Science and Technology Aerospace Doctoral Program of UPC. In January 2012, the European Space Agency granted Adrià a PhD. co-sponsorization fellowship together with the industrial partner FUGRO. Since then Adrià's research is focused in enhanced algorithms related with the real-time Fast-PPP technique. He co-authors 2 papers in peer-reviewed journals, 2 book chapters and 13 works in meeting proceedings, with 1 best presentation award from the US Institute of Navigation.

Dr. José Miguel Juan Zornoza is teaching at the UPC in Barcelona, Spain, in the Department of Applied Physics since 1988. He was granted tenure and promoted to Associate Professor in 1991. He obtained the National accreditation for Full Professor in 2011. He has published over 70 papers in peer-reviewed journals and about 200 works in meeting proceedings, with 4 best paper awards from the US Institute of Navigation. He co-authors 5 patents on GNSS and 4 books on GNSS Data Processing.

Dr. Jaume Sanz Subirana is teaching at the UPC in Barcelona, Spain, in the Department of Applied Mathematics since 1983. He was granted tenure and promoted to Associate Professor in 1988. He obtained the National accreditation for Full Professor in 2011. He has published over 70 papers in peer-reviewed journals and about 200 works in meeting proceedings, with 4 best paper awards from the US Institute of Navigation. He co-authors 5 patents on GNSS and 4 books on GNSS Data Processing.

Dr. Guillermo González-Casado is teaching in the UPC in Barcelona, in the Department of Applied Mathematics, being granted tenure and promoted to Associate Professor in 1999. His current research interests are focused in ionospheric modeling based in GNSS observations and radio occultations, Ground Based Augmentation Systems, and the study and development of GNSS applications in general. He has published about 20 papers in peer-reviewed journals and more than 25 works in meeting proceedings.

Mr. Deimos Ibáñez received the Telecommunications Engineering degree in December 2014 from the UPC, Spain. In 2013 he entered gAGE to add different ionospheric models to the gLAB tool suite. He currently maintains the tool and he is implementing SBAS capabilities to gLAB. He co-authors 7 works in meeting proceedings.

Mr. Jesús Romero Sánchez received the Bachelor of Science in Aeronautics in 2009 and the Aeronautical Engineering degree in November 2013 from the UPC, Spain. He joined gAGE in 2015 to support ongoing R+D projects. Jesús has a professional experience of more than 6 years in GNSS in both private and public Institutions.

ABSTRACT

The main objective of this work is to present a methodology to assess the accuracy of any ionospheric model used in Global Navigation Satellite System (GNSS) applications. A number of global and regional models (both in real-time and post-process) will be analyzed during the entire 2014, i.e. near to the last Solar Cycle Maximum, to identify seasonal characteristics. The new method uses as reference values the unambiguous and undifferenced geometry-free combination of carrier-phase measurements from a world-wide distribution of receivers. The differences between the Slant Total Electron Contents (STECs) of the model and the measurements are fit to constant hardware delays: a receiver plus a satellite Differential Code Bias (DCB). Once such DCBs are estimated, the post-fit residual of the adjustment to the reference values is computed. It is shown that this residual is a very suitable metric to represent the error of any ionospheric model tailored for GNSS-based navigation. Any miss-modeling present in the STECs predictions which cannot be represented by a constant parameter per station and a constant per satellite degrades the user positioning. The assessment includes the comparison of the 3D navigation error of some permanent stations, being processed in single-frequency as kinematic rovers, using different ionospheric corrections and precise satellite orbits and clocks.

BACKGROUND

Once that orbits and clocks precise to a few centimeters are available in real-time [1], the ionospheric modeling is the main limiting factor in the accuracy of single-frequency receivers. In order to take benefit of the accuracy of these precise orbit and clock products, the errors in the ionospheric correction shall not be greater than 1 Total Electron Content Unit (TECU), i.e., 16.24 cm in the L1 frequency band.

In this regard, it is of great interest a correct characterization of the accuracy of GNSS ionospheric models. This is a long-standing issue, still challenging, due to the lack of accurate enough ionospheric determinations to be used as a reference. The chosen approach overcomes the limited degree of realism of simulations, when perturbed (i.e., non-nominal) ionospheric conditions are encountered. Even quite ordinary events such as geomagnetic storms in northern latitudes or equatorial scintillation after the local sunset are difficult to be realistically simulated [2].

The methodology also improves other tests using independent Total Electron Content (TEC) measurements from dual-frequency space-borne radar altimeters like TOPEX/Jason [3]. Some authors [4] have pointed uncertainties in such measurements of at least 5 TECUs. Therefore, it is difficult to distinguish which part of the error is due to the ionospheric model and which is due to the radar-altimeter data [5]. Note that an uncertainty of 5 TECUs (i.e., totaling 0.81 cm in L1) might not be acceptable for precise navigation applications, which are targeted to a few decimeters of accuracy.

METHOD

The proposed methodology is based in the comparison between the predictions of the ionospheric model with actual undifferenced, geometry-free combination of carrier-phase GNSS measurements gathered from a world-wide distribution of permanent receivers. An example of the network is shown in Figure 1, where three different sub-sets of receivers are displayed. Red and green receivers are used to assess the real-time ionospheric corrections of the European and American Satellite-Based Augmentation System (SBAS) to the Global Positioning System (GPS), respectively. All stations are used to assess Global Ionospheric Maps (GIMs).

Thanks to the advanced modeling capabilities of the Central Processing Facility (CPF) of the Fast Precise Point Positioning (Fast-PPP) technique, developed by the first author of [6] and patented in [7], the carrier-phase ambiguities can be fixed and removed from the measurements (i.e., becoming unambiguous measurements). The error of these unambiguous, undifferenced, geometry-free combination of carrier-phase measurements is under few tenths of 1 TECU, which is several times smaller than the error of the models analyzed. Thence, it is very adequate to be used as a reference to assess ionospheric models.

The underlying idea is that differences between the model STEC predictions and the measurements shall be separated in (1) into a sort of hardware delays (a receiver constant plus a satellite constant) per data interval, e.g., a day. The condition that these hardware delays, or DCB, are commonly shared throughout the world-wide network of receivers and satellites provides a global character to the assessment. The method uses undifferenced STECs, which generalizes simple tests based on Double Difference (DD) of STECs between pairs of satellites and receivers. Such DD ionospheric tests are limited to a much more local scale, because common view of the satellites is needed. In addition to this limitation, and most important, epoch to epoch miss-modelings are canceled in the DDs because of its construction nature.

$$STEC^{j}_{model,i} - (LI^{j}_{i} - BI^{j}_{i}) = K_i + K^{j} \qquad (1)$$

The differences computed in previous equation between the modeled STECs and the measurements fed a Least Squares (LS) process to estimate the hardware delays for stations and satellites. Numerically, using 24 hours of data sampled every 30 Second of the Day (SoD) from about 150 stations globally distributed and an average of 8 satellites

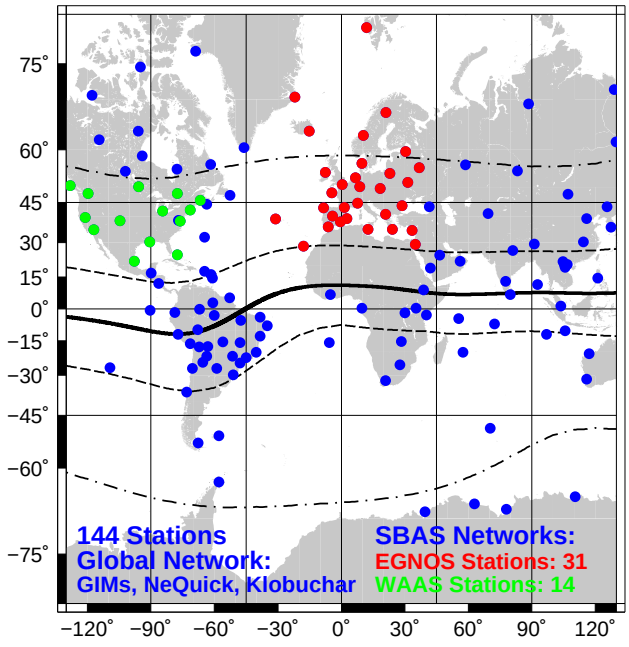

Figure 1: Distribution of permanent receivers used to assess ionospheric models during 2014. All stations participate in the assessment of global models: GIMs, Klobuchar (GPS) and NeQuick (Galileo). The red and green sub-set of receivers are used to assess the real-time ionospheric corrections of EGNOS and WAAS, respectively. The black curves indicate different MODIP latitudes: $0°$ **(solid),** $\pm 36°$ **(dashed),** $\pm 60°$**(dash-dots).**

in view per station, each day approximately 3.5 million STECs are fit to 180 parameters (150 $\hat{K}_{sta}$ + 30 $\hat{K}^{sat}$). By estimating these DCBs, any existing bias in the STECs of the model being tested is absorbed into the receiver and satellite constants. Thence, the test results are not affected by the fact that every model uses a different reference in its internal computations. Examples of these differences are: constraining to zero the DCB value for a particular station or a zero mean condition for all DCB satellites (see [8]). The results of the test are also independent to the different DCBs values determined by the geometric description of the ionospheric delay of every model [9].

Once the satellite and station DCBs are estimated as daily constants, the post-fit residuals of the adjustment to the original reference values are computed. The post-fit residuals result into a very suitable metric to represent the error of the ionospheric models tailored for satellite-based navigation. Indeed, any miss-modeling of the STECs predicted by any ionospheric model that cannot be represented by a constant parameter per station and a constant per satellite, result in a degradation of the user positioning. These miss-modelings are sampled in the post-fit residuals.

$$RES^{j}_{model,i} = STEC^{j}_{model,i} - (LI^{j}_{i} - BI^{j}_{i}) - (\hat{K}_i + \hat{K}^{j}) \qquad (2)$$

In order to compare the post-fit residuals obtained for each ionospheric model under test in a better manner, it is

proposed to compute the Root Mean Square (RMS) for all the STECs for all satellites in view per station per all the stations following:

$$RMS_{model} = \sqrt{\frac{1}{n_{STEC}} \sum_{i=1}^{n_{sta}} \sum_{j=1}^{n_{sat(i)}} \left(RES^{j}_{model,i} \right)^2} \quad (3)$$

Where n_{STEC} equals the total number of STECs for the period for which the RMS is computed. The value depends on the number of stations, n_{sta}, and the number of satellites seen by every station, n_{sat}, during the RMS interval (typically one hour). Notice that the chosen metric is a RMS, meaning that errors several times larger than the RMS are not unusual, especially at Local Times (LTs) around mid-day, at stations at equatorial latitudes, and for low-elevation observations.

Reference Data

The necessary products needed to apply the proposed test to any model prediction are being disseminated for the GNSS community via an Internet server accessible in www.gage.upc.edu/products. In this address one can find the guidelines for the correct usage of these products. This eliminates the complex data processing explained in the previous section.

Three types of reference products are available on every Day of Year (DoY) with different data for each satellite (hereafter identified with the Pseudo-Random Noise (PRN) and the constellation identifier). First, the file named "**gage**yyyyddd.**stec**" with the unambiguous and unbiased $L1 - L2$ combination of carrier-phase measurements (i.e., the true STECs) for the entire network of stations. Second, the "**gage**yyyyddd.**bias**" with the satellite DCB together with its standard deviation in meters of P2-P1 and the fractional part of the ambiguities in the Wide Lane (WL) combination (BW) and in the f_1 frequency (B1), in cycles, (see [10] for notation details). The third product the "**gage**0ddd.yy**i**" is a two-layer GIM stored as a IONosphere map EXchange format (IONEX) standard [11]. The description of the non-standard products (i.e., the biases and true STECs) can be found in Table I.

TABLE I. Description of the content of the reference products

File Type	Content Description	Field Units
bias	Epoch (Year, DoY, SoD)	GPS Time
	GNSS Satellite	PRN Number
	Fractional B1 Fractional BW	cycles
	Satellite DCB DCB Standard deviation	meters of P2-P1 delay
stec	Epoch (Year, DoY, SoD)	GPS Time
	Station Name	-
	GNSS Satellite	PRN Number
	Arch Number	-
	Satellite Elevation	degrees
	Line Of Sight vector	-
	LI-BI	meters of L1-L2 delay
	P2-P1	meters of P2-P1 delay

Performance Results

The ionospheric references previously detailed have been used during the entire 2014, i.e., near to the last Solar Cycle Maximum, to characterize the accuracy of different ionospheric models currently used in GNSS. The assessment includes the operational models broadcast in real-time by the GPS and Galileo constellations [12], [13] and their correspondent SBAS. In this sense, the performance of the NeQuick (Galileo) [14] and Klobuchar (GPS) [15] models is assessed globally. On a regional scale, the ionospheric corrections of Wide Area Augmentation System (WAAS) and European Geostationary Navigation Overlay System (EGNOS) are also examined, after applying the Minimum Operational Performance Standards (MOPS) [16] in the areas defined by CONtiguous United States (CONUS) and the European Civil Aviation Conference (ECAC) [17], respectively.

Figure 2 depicts the RMS of the post-fit residuals (i.e., the error) of the STECs modeled with the operational models along the year for different MOdified DIP latitudes (MODIPs) [18]. The results of the global models are displayed in the top row using a scale of 0-35 TECUs, for GPS on the left column and Galileo on the right column. The largest errors occur near the March and September Equinoxes, whereas the lowest errors take place around June and December Solstices. It can be seen that NeQuick (Galileo) or Klobuchar (GPS) predictions can range from 8 TECUs at mid-latitude regions to more than 20 TECUs at low latitudes. In relative terms, the error of NeQuick-GAL is 30% and Klobuchar 35% of the total slant delay.

The RMS of the post-fit residuals for the SBASs ionospheric corrections is depicted in the bottom row of Figure 2, using a scale of 0-16 TECUs. The depicted post-fit residuals are smaller than the global models because SBASs operate at middle latitudes (i.e., excluding equatorial areas) and using a shorter time-update rate of 5 minutes. EGNOS and WAAS performance is similar when it is compared on the same MODIP basis, with errors between 2 to 4 TECUs, which represent around the 10% of the total slant delay. It can be seen that EGNOS includes a more equatorial MODIP band which concentrates larger errors up to 10 TECUs.

The methodology has been applied also to GIMs obtained in post-process. Figure 3 shows the RMS of the post-fit residual errors using a scale of 0-16 TECUs, except for the Fast-PPP model (described in [6], [19]), which is 0-1 TECU. The top left plot depicts the post-fit residuals of the Rapid Product of the International GNSS Service (IGS) [20], updated every 2 hours. The errors range from around 3 TECUs at mid-latitude to around 16 TECUs for equatorial latitudes. In average, this corresponds to a 15% modeling error. Notice that the test is done over oblique STECs, so this result is fully compatible with the published IGS-GIMs nominal accuracy of 2-8 TECU, for the Vertical Total Electron Content (VTEC) [21].

The top right plot of Figure 3 shows the RMS of the post-fit residuals of the real-time (i.e., forward-only) Fast-

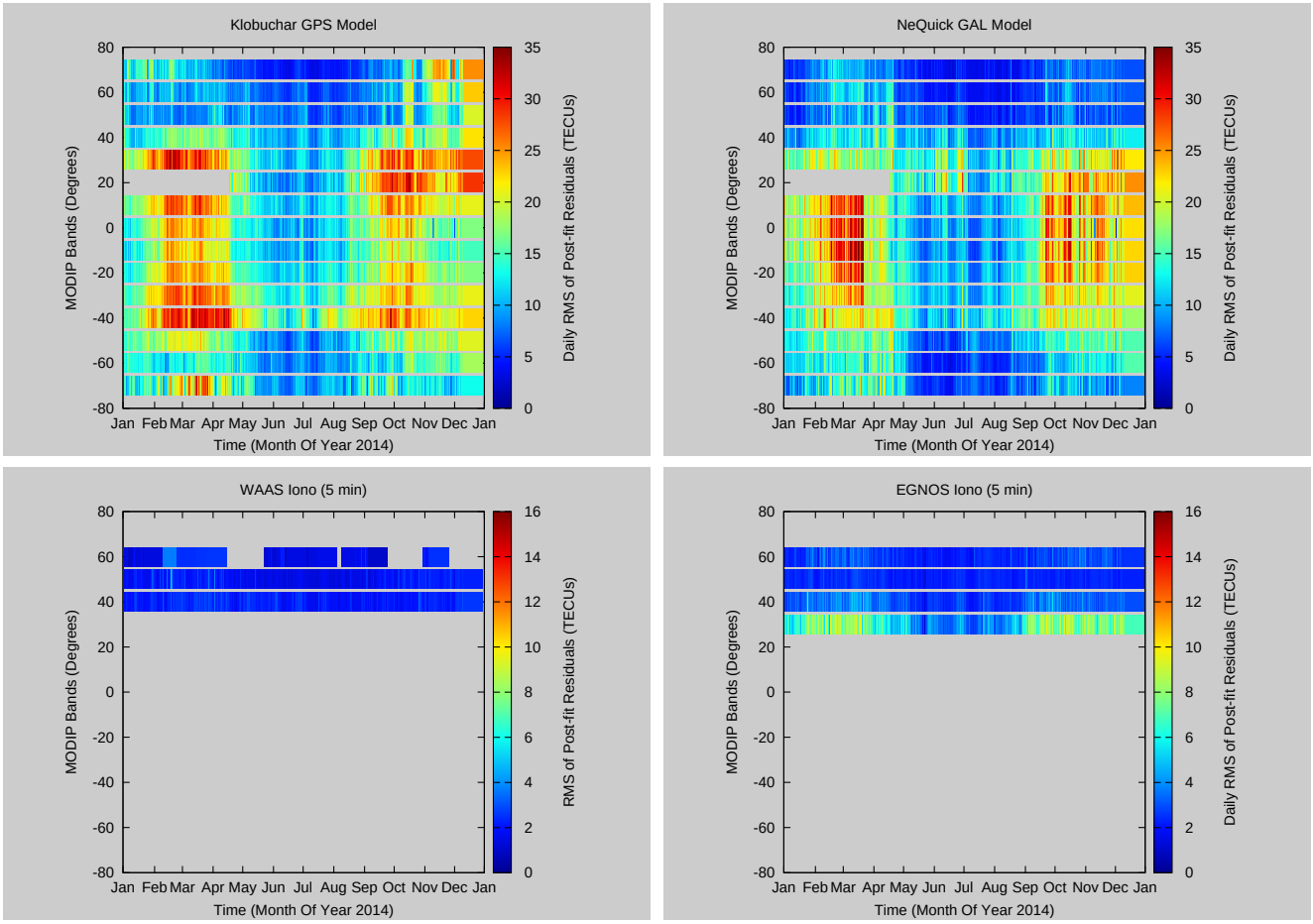

Figure 2: Results of the consistency test between different operational GNSS ionospheric models along year 2014 for different MODIP latitudes. The top row shows the absolute value of the error of the GPS (left) and NeQuick Galileo (right) broadcast models, while the bottom row represents the real-time (5 min) ionospheric corrections of the augmentation systems WAAS (left) and EGNOS (right). The color band in every plot indicates the range of the errors.

PPP two-layer [22] model at the level of less than 1 TECU. This accuracy is achieved thanks to:

- It uses ambiguity-fixed carrier-phase measurements, instead of code-leveled [23] carrier-phases.
- The time resolution (5 minutes) is adequate to reproduce the temporal variation of the ionosphere.
- The two-layers description of the ionospheric delay instead of single-layer approach, which is important especially in the equator.
- The usage of the MODIP latitude (instead of geographical) increases the resolution in the areas where the ionospheric gradients are large.

The real-time Fast-PPP model is smoothed (both in time and space) in poorly sounded areas (e.g., oceans). In this way, the smoothed (but with global coverage) Fast-PPP GIMs are generated every 15 minutes. The post-fit residual error of the Fast-PPP GIMs is shown in the bottom row of Figure 3. The advantage of interpolating using the MODIP latitude (bottom-right) instead of the geographical latitude (bottom left) confirms previous studies (see for instance [24]). The enhancement is especially noticeable in the equatorial areas within the $\pm 36^{\circ}$ of MODIP (see the dashed line in Fig. 1). In average, the Fast-PPP GIM shows a typical error of its STEC predictions around 1 to 2 TECUs, maintained also at low latitude regions. This corresponds approximately to a modeling error of the 5% of the total slant delay.

Table II summarizes the results of the test in a numerical manner, allowing a better comparison across different ionospheric models. In every row, the RMS of the post-fit residuals is computed on a monthly basis. The last row represents the average RMS for all year 2014. The relative error with respect to the total slant ionospheric delay is computed after dividing every RMS by the $LI - BI$ (i.e., the true STEC). It is noticeable that the relative errors are more constant than the absolute magnitudes.

Table II shows that the global operational models of Galileo and GPS present relative errors to the total slant delay about 30% to 40% along the year, with average percentages 30% and 36%, respectively. The real-time, regional ionospheric corrections of SBAS are more accurate than the global models, with relative errors in the range 5% to 14%,

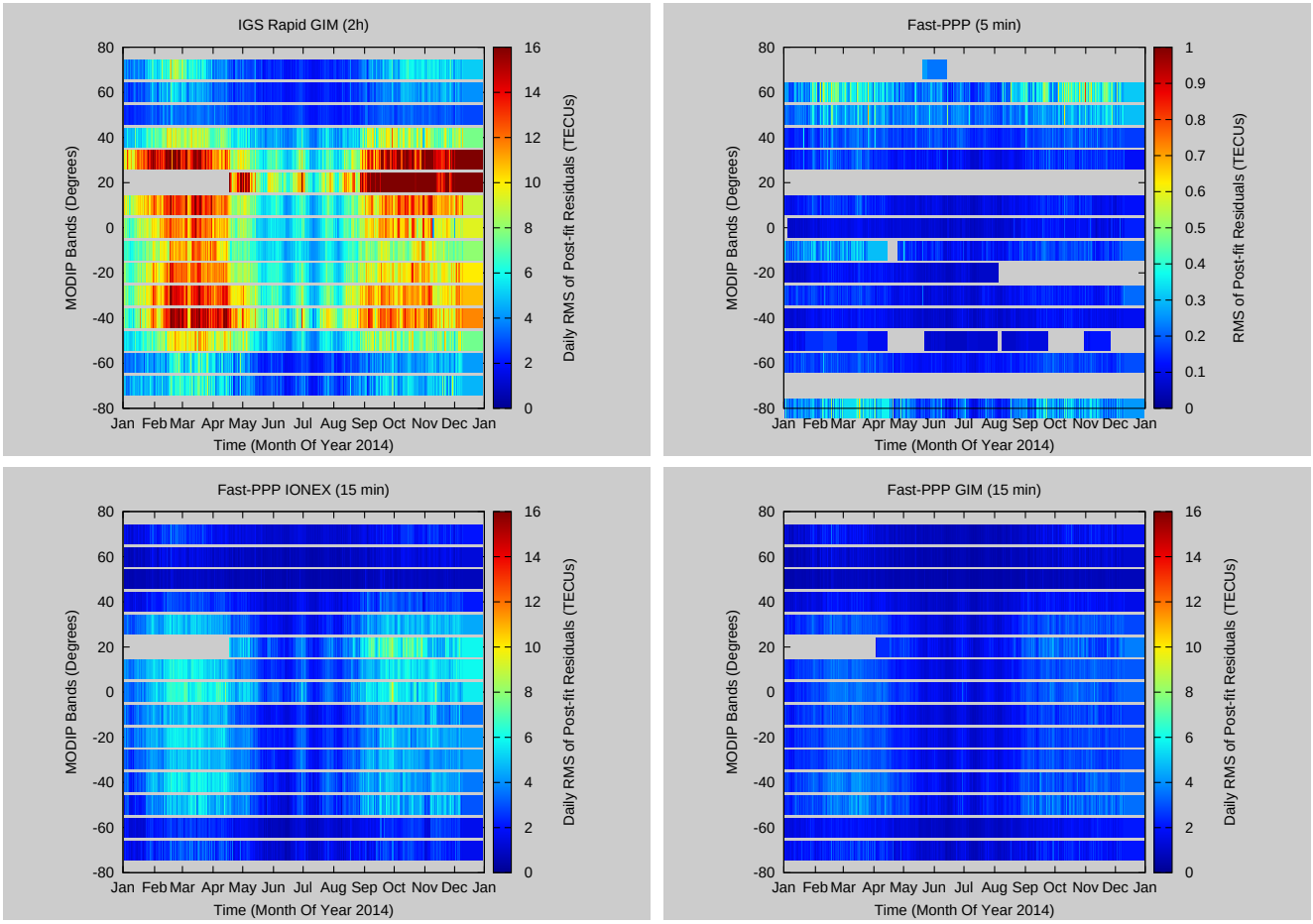

Figure 3: Results of the consistency test between different GNSS ionospheric models along year 2014 for different MODIP latitudes. The upper left plot corresponds to the 2-h Rapid IGS GIM, the upper right plot to the real-time 5-min two-layer Fast-PPP model. In the bottom row, the 15 min Fast-PPP GIM are stored in IONEX format (left, geographical latitude interpolation) and using the MODIP interpolation (right). The color band in every plot indicates the range of the errors.

on average, 6% and 9% for WAAS and EGNOS, respectively. Finally, the post-processed global Rapid Product of the IGS presents a relative post-fit residual errors in the range from 13% to 19%, with an average of 16.40%.

Table II also presents the different Fast-PPP determinations. The real-time forward-only model presents a negligible error of 0.48% of the total slant delay. The temporal and spatial smoothings applied to build the post-process Fast-PPP GIM enlarge the post-fit residuals of the real-time Fast-PPP model by one order of magnitude, ranging 3% to 5%, and on average the 4.39% of the total slant delay. The contribution of the latitude interpolation to the final error can be inferred by comparing the post-fit residual errors of the Fast-PPP GIMs when stored using a MODIP format with respect to the IONEX standard. The Fast-PPP IONEX present relative errors in the range of 5% to 7%, with a year average error of 6.38% of the total slant delay.

Assessment on the Navigation Domain

After having discussed the test results on the ionospheric assessment, this section is devoted to show how the accuracy of the ionospheric modeling is translated to the user domain, specifically, to the single-frequency navigation. For this purpose, two permanent stations are selected within the ECAC area. The first one, named **ebre**, is located in mid-latitude with geographical coordinates (00°E 41°N) and 48°of MODIP. The second one, named **izan**, is located in a more equatorial area with geographical coordinates (16°W 28°N) and 35°of MODIP.

In order to assess the impact of different ionospheric conditions, two different DoYs are selected according to the results of previous section. On one hand, DoY 165 (June), when all the models present lowest post-fit residuals errors. On the other, DoY 318 (November), when the post-fit residuals of the models are maximum. The level of ionospheric activity of both DoYs can be compared using the RMS of the Along Arc TEC Rate (AATR) [25]. The AATR particularly samples the lack of linearity of the ionosphere which is assumed by all ionospheric models. The greater the AATR, the greater the error of the ionospheric corrections, and finally, a worsening of the navigation solution occurs.

Table III shows the maximum RMS of the AATR over one hour for the two selected rovers at the two DoYs. The AATRs for the low-latitude rover **izan** are 50% greater than

TABLE II. POST-FIT RESIDUAL ERRORS FOR GLOBAL (LEFT) AND REGIONAL (RIGHT) IONOSPHERIC MODELS IN TECU AND RELATIVE TO THE STEC

Month	GPS		Galileo		Fast-PPP RT		Fast-PPP GIM		Fast-PPP IONEX		IGS-GIM		WAAS		EGNOS	
	RMS	(%)	RMS	(%)	RMS	(%)	RMS	(%)	RMS	(%)	RMS	(%)	RMS	(%)	RMS	(%)
January	14.60	42.17	11.71	33.80	0.18	0.52	1.75	5.05	2.19	6.32	5.92	17.10	1.92	9.18	2.86	14.01
February	17.61	37.44	15.14	32.22	0.22	0.48	2.18	4.62	3.27	6.93	8.38	17.77	2.26	6.41	3.33	10.46
March	19.00	32.31	17.67	30.07	0.23	0.39	2.47	4.20	3.72	6.34	9.34	15.87	2.29	4.78	3.56	7.44
April	17.53	34.77	15.15	30.66	0.21	0.41	2.15	4.26	3.30	6.57	8.17	16.20	2.29	5.54	3.11	7.42
May	12.61	32.16	9.97	25.40	0.16	0.42	1.52	3.86	2.35	5.95	5.85	14.82	1.86	5.19	2.49	6.94
June	9.35	29.75	8.78	28.17	0.16	0.51	1.10	3.46	1.43	4.54	4.23	13.38	1.67	5.33	2.36	7.22
July	9.72	31.11	8.34	26.62	0.15	0.48	1.14	3.61	1.73	5.46	4.40	14.00	1.69	5.59	2.47	7.77
August	11.08	35.31	8.49	27.12	0.15	0.47	1.30	4.13	1.97	6.26	5.00	15.88	1.65	6.17	2.45	8.74
September	14.54	35.55	11.10	27.16	0.20	0.48	1.95	4.79	2.95	7.22	7.21	17.61	1.85	5.91	2.98	9.41
October	18.02	38.81	14.85	32.01	0.22	0.48	2.14	4.61	3.26	7.04	7.96	17.19	2.08	6.14	3.16	9.39
November	17.60	39.42	14.38	32.07	0.23	0.52	2.16	4.83	3.08	6.90	7.91	17.64	2.29	6.99	3.11	10.43
December	16.56	41.97	13.66	34.65	0.23	0.58	2.08	5.28	2.83	7.17	7.59	19.26	2.30	7.89	3.03	12.15
Average	14.85	35.90	12.44	30.00	0.20	0.48	1.83	4.39	2.67	6.39	6.83	16.40	2.01	6.26	2.91	9.28

the mid-latitude **ebre** rover for every DoY, indicating that **izan** is located in a more challenging ionospheric location. It is also noticeable that the AATRs of DoY 318 are three times larger than in DoY 165 for both rovers. The AATR results are in line with the RMS of the post-fit residuals of the ionospheric test shown in Table IV applied at the nearest station used to derive the Fast-PPP ionospheric model with respect to the presented rovers; the rover **izan** is located at 146 kilometers from lpal station and rover **ebre** 230 kilometers to mall station.

The assessment of the navigation results has been done as follows. The selected permanent stations are treated as pure kinematic rovers, computing their navigation solution every 30 seconds during 24 hours of actual GNSS data collection. Every 2 hours, the navigation filter of the rover is reset to have 12 windows of independent solutions per day. Then, the RMS of the 3-D navigation error is computed merging all resets in the same plot, as a function of the time elapsed since the last reset of the navigation filter. Every plot shows the solution of the rovers with the ionospheric delay being corrected with the determinations of IGS-GIM, EGNOS and Fast-PPP GIM. In order to have a reference result, it is also included the ionospheric-free Group and Phase Ionospheric Calibration (GRAPHIC) solution described in [26]. It is worth to mention that the same precise satellite orbits and clocks are used, for each corresponding DoY.

Figure 4 shows the single-frequency navigation results for the two different DoYs. It is worth first to analyze the reference GRAPHIC solution displayed in black in both rovers, because does not depend on the ionospheric conditions and only on the noise of the pseudorange measurements at the receivers. It can be seen that the receiver at **ebre** (top) presents a noisier solution than the **izan** receiver (bottom). The final accuracy at the end of the two hour resetting window is almost converged in **izan**, while still decreasing in **ebre**. The final RMS 3-D errors are similar at the middle of the year solution (left) and at the end of year (right), about 40 and 20 centimeters, at **ebre** and **izan**, respectively. The navigation solutions that are using ionospheric information reduce the convergence time to the final GRAPHIC accuracy if: i) the ionospheric information is free of miss-modeling, ii) the actual error of the ionospheric corrections are realistically bounded by associated the formal error used to weight the ionosphere in the navigation filter [19].

TABLE III. MAXIMUM RMS AATR AT THE ROVER STATIONS OVER ONE HOUR IN UNITS OF MM/S IN THE L1 FREQUENCY

rover		AATR	
name	latitude	DoY 165	DoY 318
ebre	41°N	0.4	1.2
izan	28°N	0.6	1.8

TABLE IV. DAILY POST-FIT RESIDUAL ERRORS AT THE REFERENCE STATIONS FOR DIFFERENT IONOSPHERIC MODELS IN UNITS OF TECU

reference		Fast-PPP GIM		EGNOS		IGS GIM	
name	latitude	DoY 165	DoY 318	DoY 165	DoY 318	DoY 165	DoY 318
mall	39°N	0.83	0.89	2.14	2.56	3.26	4.60
lpal	29°N	2.41	3.09	3.46	8.83	5.97	18.00

Figure 4 shows in blue the RMS of the 3-D errors of the navigation solution using the Fast-PPP GIMs. This single-frequency Fast-PPP solution converges several times faster to the same final ionosphere-free accuracy of GRAPHIC thanks to the two conditions previously mentioned. The RMS of the 3-D errors are sub-metric from the start at both rovers and at the two DoYs. This result agrees with Figure 3, proving the capability of the Fast-PPP GIM to adapt to the actual ionospheric conditions along the year.

The RMS of the 3-D error of the navigation solution with the EGNOS ionosphere is shown in red. A greater variability of the navigation solution is observed. In **ebre**, the final accuracy is comparable to the GRAPHIC solution, but it is not the case for the low-latitude **izan** rover. This is mainly attributable to the increasing miss-modeling of the single-layer approach with lower latitudes, which underestimates the interaction between the equatorial ionosphere and the mid-latitude plasmasphere.

Finally, it is also depicted in green the RMS of the 3-D error of the navigation solution using the IGS-GIM ionosphere. It can be seen that the navigation results are affected not only from the single-layer approach, but also from its lower time-update (two hours) and the smoothing applied in its determination. This is especially noticeable in the low-latitude rover receiver **izan**.

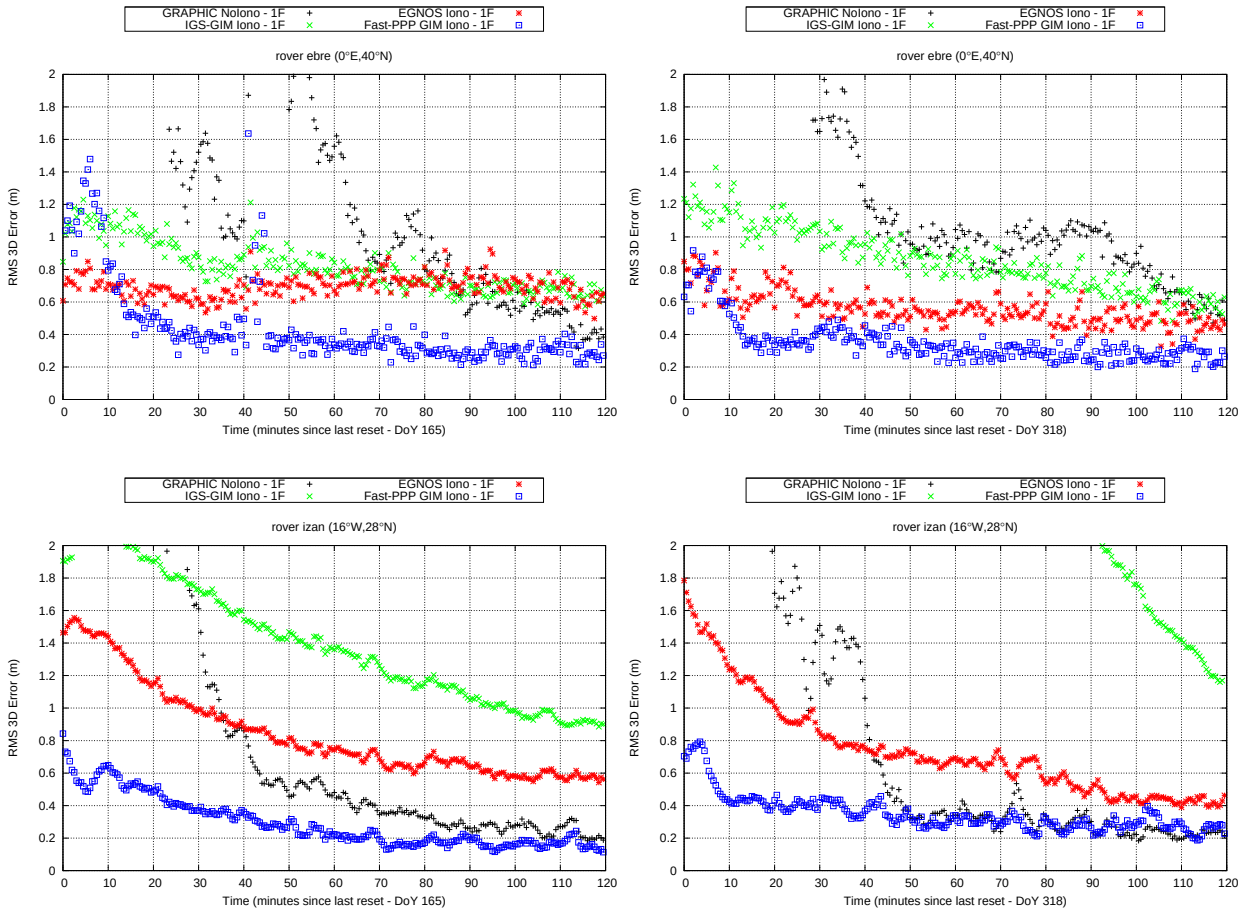

Figure 4: Single-Frequency Navigation results: RMS of the 3-D error as a function of time since the user receiver is reset (with resets every 2 hours and 12 resets merged per day) for rover ebre (top) and izan (bottom) for DoY 165 (left) and 318 (right) of year 2014. In each plot, the ionosphere-free single-frequency solution GRAPHIC (black) is compared with the enhanced positioning using the ionospheric determinations from the Fast-PPP GIM (blue), IGS-GIMs (green) and EGNOS (red).

CONCLUSIONS

A methodology for the assessment of the accuracy of ionospheric models for GNSS has been summarized in this work, together with its application to the main ionospheric models used nowadays. The results suggest that state of the art ionospheric models can be improved by using the proposed methodology in conjunction with precise STEC determinations. In this regard, the unambiguous, unbiased STECs calculated for 2014 by the Research group of Astronomy and Geomatics have been upload to a publicly-available server at www.gage.upc.edu/products for its dissemination.

The findings underline that the temporal resolution of the techniques considered does not solely explain the different performances. Indeed, other factors of greater importance have been found. In particular, the process noise in the model generation, the amount of spatial and temporal smoothing needed to cover all the globe, the model geometry (e.g., the grid resolution), the chosen representation of the latitudinal variations and, finally, the number of layers to model the different behavior of the components in the ionosphere. These error contributions have been assessed in the generation of the Fast-PPP GIM from the real-time Fast-PPP model.

The exposed methodology complements other analysis based on the comparison of the navigation achieved using different sources of ionospheric corrections. Indeed, with routinely real-time precise orbits and clocks, the modeling accuracy of ionosphere is the limiting factor of single-frequency receivers (e.g., the mass-market). It has been shown that the 3-D positioning error of the single-frequency navigation can range from meter-level when the IGS GIMs, to the decimeter-level of accuracy when the determinations of EGNOS (regional) or Fast-PPP (global), are used instead.

ACKNOWLEDGMENTS

The authors acknowledge the use of data from the International GNSS Service. This work has been partially sponsored by the European Space Agency through an Networking/Partnering Initiative grant with the industrial partner FUGRO. The Technical University of Catalonia contributed with an FPI-UPC grant. The work has been done in the context of the project Ionospheric Conditions and Associated Scenarios for EGNOS (ICASES) [27].

DISCLAIMER

The Research group of Astronomy and Geomatics (gAGE) at the Technical University of Catalonia (UPC) specifically disclaims liability for any incidental or consequential damages and assumes no responsibility or liability for any loss or damage suffered by any person or third party as a result of the use or misuse of any of the information or content on the website www.gage.upc.edu/products. The reference products are intended for scientific purposes only, expecting a proper citation whenever these products are used.

REFERENCES

[1] T. Murfin, "Look, No Base-Station! Precise Point Positioning (PPP)." 2013. [Online]. Available: http://gpsworld.com/look-no-base-station-precise-point-positioning-ppp

[2] G. S. Bust and C. N. Mitchell, "History, current state, and future directions of ionospheric imaging," *Reviews of Geophysics*, vol. 46, no. 1, pp. n/a–n/a, 2008. [Online]. Available: http://dx.doi.org/10.1029/2006RG000212

[3] L.-L. Fu, E. J. Christensen, C. A. Yamarone, M. Lefebvre, Y. Mnard, M. Dorrer, and P. Escudier, "TOPEX/POSEIDON mission overview," *Journal of Geophysical Research: Oceans*, vol. 99, no. 12, pp. 24 369–24 381, 1994. [Online]. Available: http://dx.doi.org/10.1029/94JC01761

[4] G. Jee, H.-B. Lee, Y. H. Kim, J.-K. Chung, and J. Cho, "Assessment of gps global ionosphere maps (gim) by comparison between code gim and topex/jason tec data: Ionospheric perspective," *Journal of Geophysical Research: Space Physics*, vol. 115, no. A10, 2010. [Online]. Available: http://dx.doi.org/10.1029/2010JA015432

[5] D. A. Imel, "Evaluation of the TOPEX/POSEIDON dual-frequency ionosphere correction," *Journal of Geophysical Research: Oceans*, vol. 99, no. C12, pp. 24 895–24 906, 1994. [Online]. Available: http://dx.doi.org/10.1029/94JC01869

[6] J. Juan, M. Hernández-Pajares, J. Sanz, P. Ramos-Bosch, A. Aragon-Angel, R. Orus, W. Ochieng, S. Feng, P. Coutinho, J. Samson, and M. Tossaint, "Enhanced Precise Point Positioning for GNSS Users." *IEEE Transactions on Geoscience and Remote Sensing*, 2012. [Online]. Available: http://dx.doi.org/10.1109/TGRS.2012.2189888

[7] M. Hernández-Pajares, J. Juan, J. Sanz, J. Samson, and M. Tossaint, "Method, Apparatus and System for Determining a Position of an Object Having a Global Navigation Satellite System Receiver by Processing Undifferenced Data Like Carrier Phase Measurements and External Products Like Ionosphere Data. international patent application PCT/EP2011/001512 (ESA ref.: ESA/PAT/566)." 2011. [Online]. Available: https://patentscope.wipo.int/search/en/detail.jsf?docId=WO2012130252&recNum=76&docAn=EP2011001512&queryString=&maxRec=127507

[8] O. Montenbruck, A. Hauschild, and P. Steigenberger, "Differential Code Bias Estimation using Multi-GNSS Observations and Global Ionosphere Maps," *Navigation*, vol. 61, no. 3, pp. 191–201, 2014. [Online]. Available: http://dx.doi.org/10.1002/navi.64

[9] A. J. Mannucci, B. D. Wilson, D. N. Yuan, C. H. Ho, U. J. Lindqwister, and T. F. Runge, "A global mapping technique for gps-derived ionospheric total electron content measurements," *Radio Science*, vol. 33, no. 3, pp. 565–582, 1998. [Online]. Available: http://dx.doi.org/10.1029/97RS02707

[10] J. Sanz, J. Juan, and M. Hernández-Pajares, GNSS Data Processing, Vol. I: Fundamentals and Algorithms. Noordwijk, the Netherlands: ESA Communications, ESTEC TM-23/1, 2013. [Online]. Available: http://www.navipedia.net/GNSS_Book/ESA_GNSS-Book_TM-23_Vol_I.pdf

[11] S. Schaer, W. Gurtner, and J. Feltens, "IONEX: The IONosphere Map Exchange Format Version 1," in *Proceeding of the IGS AC Workshop*, Darmstadt, Germany, Feb. 1998, pp. 233–247. [Online]. Available: https://igscb.jpl.nasa.gov/igscb/data/format/ionex1.pdf

[12] IS-GPS-200, "GPS Interface Specification IS-GPS-200. Revision E." 2010. [Online]. Available: http://www.gps.gov/technical/icwg/IS-GPS-200E.pdf

[13] Galileo SIS ICD, EU, "Galileo Open Service Signal In Space Control Document (OS SIS IDC), Issue 1.1." 2010. [Online]. Available: http://ec.europa.eu/enterprise/policies/satnav/galileo/open-service/index_en.htm

[14] G. Di Giovanni and S. Radicella, "An Analytical Model of the Electron Density Profile in the Ionosphere." Advances in Space Research, vol. 10, no. 11, pp. 27–30, 1990. [Online]. Available: http://dx.doi.org/10.1016/0273-1177(90)90301-F

[15] J. Klobuchar, "Ionospheric time-delay algorithm for single-frequency gps users," *Aerospace and Electronic Systems, IEEE Transactions on*, vol. AES-23, no. 3, pp. 325–331, May 1987. [Online]. Available: http://dx.doi.org/10.1109/TAES.1987.310829

[16] RTCA, "Minimum Operational Performance Standards for Global Positioning System/Wide Area Augmentation System Airborne Equipment.rtca document 229-C," Washington, USA, 2006.

[17] "Constitution and Rules of Procedure of the European Civil Aviation Conference (ECAC)," Dec. 1955.

[18] K. Rawer, *Propagation of Decameter Waves (HF-band) in Meteorological and Astronomical Influences on Radio Wave Propagation*. New York: Ed. Landmark, B. Pergamon Press, 1963.

[19] A. Rovira-Garcia, J. Juan, J. Sanz, and G. Gonzalez-Casado, "A worldwide ionospheric model for fast precise point positioning," *Geoscience and Remote Sensing, IEEE Transactions on*, vol. 53, no. 8, pp. 4596–4604, Aug 2015. [Online]. Available: http://dx.doi.org/10.1109/TGRS.2015.2402598

[20] G. Beutler, M. Rothacher, S. Schaer, T. Springer, J. Kouba, and R. Neilan, "The International GPS Service (IGS): An interdisciplinary service in support of Earth sciences." *Advances in Space Research*, vol. 23, no. 4, pp. 631–653, 1999. [Online]. Available: http://dx.doi.org/10.1016/S0273-1177(99)00160-X

[21] International GNSS Service Products, Jan. 2014. [Online]. Available: http://www.igs.org/products/data

[22] J. Juan, A. Rius, M. Hernández-Pajares, and J. Sanz, "A two-layer model of the ionosphere using global positioning system data," *Geophysical Research Letters*, vol. 24, no. 4, pp. 393–396, 1997. [Online]. Available: http://dx.doi.org/10.1029/97GL00092

[23] L. Ciraolo, F. Azpilicueta, C. Brunini, A. Meza, and S. Radicella, "Calibration errors on experimental slant total electron content (tec) determined with gps," *Journal of Geodesy*, vol. 81, no. 2, pp. 111–120, 2007. [Online]. Available: http://dx.doi.org/10.1007/s00190-006-0093-1

[24] F. Azpilicueta, C. Brunini, and S. Radicella, "Global ionospheric maps from GPS observations using MODIP latitude," *Advances in Space Research*, vol. 38, no. 11, pp. 2324 – 2331, 2006. [Online]. Available: http://dx.doi.org/10.1016/j.asr.2005.07.069

[25] J. Sanz, J. Juan, G. González-Casado, R. Prieto-Cerdeira, S. S., and R. Orús, "Novel Ionospheric Activity Indicator Specifically Tailored for GNSS Users," in *Proceedings of ION GNSS+ 2014*, Tampa, Florida (USA), Sep. 2014, pp. 1173–1182. [Online]. Available: http://www.ion.org/publications/abstract.cfm?jp=p&articleID=12269

[26] T. P. Yunck, "Coping with the atmosphere and ionosphere in precise satellite and ground positioning," *Environmental Effects on Spacecraft Positioning and Trajectories*, vol. 73, pp. 1–16, 1993. [Online]. Available: http://dx.doi.org/10.1029/GM073p0001

[27] ESA, "ICASES: Ionospheric Conditions and Associated Scenarios for EGNOS Selected from the last Solar Cycle. PO1520026618/01." Noordwick, The Netherlands, 2014.